The Polarization of Polycyclic Aromatic Hydrocarbons Curved by Pentagon Incorporation: The Role of the Flexoelectric Dipole

Jacob W. Martin,[†] Radomir I. Slavchov,[†] Edward K. Y. Yapp,[†] Jethro Akroyd,[†] Sebastian Mosbach,[†] and Markus Kraft[*,†,‡,¶]

[†]*Department of Chemical Engineering and Biotechnology, University of Cambridge, Cambridge CB3 0AS,UK*

[‡]*School of Chemical and Biomedical Engineering, Nanyang Technological University, Singapore 637459*

[¶]*Current address: West Site, Philippa Fawcett Drive, Cambridge CB3 0AS, UK*

E-mail: mk306@cam.ac.uk

Phone: +44 (0)1223 762784

Abstract

Curvature in polyaromatic hydrocarbons (PAHs), due to pentagon inclusion, produces a dipole moment that contributes significantly to self-assembly processes and adsorption at the surface of carbon materials containing curved structures. This work presents electronic structure calculations of the dipole moment for 18 different curved PAH molecules for various numbers of pentagons and the total number of aromatic rings. A significant dipole moment was found that depends strongly on the number of aromatic rings (4–6.5 debye for ring count 10–20). The main cause for the dipole is shown to be the π-electron flexoelectric effect. An atom-centered partial charge representation of the charge distribution in these molecules is insufficient to correctly describe their electrostatic potential; distributed multipoles were required instead.

Introduction

Fullerene-like curved polyaromatic hydrocarbon (PAH) fragments are known to be important intermediaries in the combustion synthesis of fullerenes and have been suggested to make up the nanostructure of soot and activated carbon.[1–4] Fullerenes can be formed in flames at low pressures[5] and curved fragments, such as corannulene (Figure 1, structure **1a**), have been extracted from soot.[6] In our recent transmission electron microscopy (TEM) studies of soot we observed curved and completely closed graphitic structures (fringes).[7] TEM fringes also were observed in synthetic soot made of hexabenzocoronene, a flat PAH, but the fringes from natural soot are of apparently higher curvature.[8] Recent kinetic Monte Carlo simulation of combustion synthesis of PAH with curvature integration showed degrees of curvature similar to that observed with TEM images, with curved PAH containing one to three pentagons.[1] Alongside soot, curved arenes have been shown to be present in activated carbon imaged using aberration-corrected TEM.[4] In glassy carbon,[9] closed fringes resembling icosahedral fullerenes have also been observed. These fullerene-like fragments have been suggested to provide the large surface area-to-volume ratio of activated carbon.[10,11] A potential formation

mechanism has been experimentally investigated where addition of methyl radicals to a pentagonal ring leads to the formation of corannulene, the C_1/C_2 formation mechanism.[12] For larger PAH molecules, introduction of pentagons through pyrolysis of a bay-site or oxidation of a zigzag edge has been suggested.[2,3,13]

The introduction of curvature into a hexagonal carbon lattice through a pentagonal point defect gives rise to a considerable molecular dipole moment. For example, corannulene (the first curved PAH to be synthesized[14]) was found experimentally to contain a dipole moment of 2.071 D[15] which is on the order of the dipole of water (1.85 D[16]). A range of indeno-corannulenes have been synthesized[17] and electronic structure calculations suggested dipole moments from 3 to 4.5 D for PAH with eight to ten rings.[18] The nm-sized curved arenes known as nanocones, with curved nuclei that grow into large graphitic cones, have been fabricated with a clear number of pentagons integrated into the nucleus/tip of the nanocone.[19,20] Electronic structure calculations of these nanocones showed a significant dipole for nanocones 0.5–4 nm in size ranging from 10 to 35 D.[21] In another study, a (10,10)-nanotube cap has been calculated to possess a dipole moment of 3.5 D.[22]

Many applications that make use of the dipole moment are being explored for these molecules – for example, the flexoelectric response of nanocones has been investigated.[21] Large nanocones have been found to self-assemble into long filaments in an electric field, which have been used to increase the conductivity between the electrodes.[23] Some curved PAHs, such as sumanene (Figure 1-**3a**), form crystal structures with 1D stacking[18] and have been suggested to possess a strong non-linear response for optical elements[24] and electronic transport properties for organic light emitting diodes.[25] The dipole moment is responsible for significant binding of curved PAH to metals which has been investigated as a method for electrical coupling between metals and organics in molecular electronics[17,26] and also could improve ion capacity in lithium ion batteries.[27]

The purpose of this paper is to calculate the dipole moment for a range of curved PAH molecules, determine the origin of the dipole moment and develop an atom-centered dis-

tributed multipole model of the electrostatic potential controlling the intermolecular interactions. This is a necessary step towards the parameterization of force fields needed for molecular dynamic simulations of systems containing curved PAHs, where the curvature-induced dipole produces the major long-range interactions and contributes significantly to the contact interactions between these molecules.

Computational Methods

A representative collection of known curved PAHs were chosen to give a range of different geometries for analysis. Their curvature is due to pentagon inclusion and produces a dipole moment. We chose structures in the size range of 10–20 rings, as these have been observed in non-graphitizing carbon as determined from fringe analysis.[4,7,28] The set contains only molecules that fulfil the isolated pentagon rule formulated for fullerenes, according to which neighboring pentagons are thermodynamically unstable and rearrange or expel C_2 to form pentagons isolated by hexagons.[29] Pericondensed PAHs with high symmetry containing only sp^2 carbon atoms have been found to be stable due to π-delocalization and are considered to be the primary species in high temperature amorphous carbons[30] and comprise the main part of the list in Figure 1 accordingly. Sumanene (**3a**) and (**3b**) contain sp^3 carbons and were also considered as they have been synthesized previously.[31,32] We shall refer to the terminating carbon atoms bonded to the hydrogen as *rim carbon* atoms and to the central carbon atoms as *hub* atoms.

The calculation of the dipole moment of a molecule requires accurate molecular geometry and electron density distribution. The hybrid density functional B3LYP[39–41] has been found to accurately describe both the geometry and the electron density of polyarenes and corannulene compared with experimentally determined values from synchrotron experiments.[42,43] Another study showed the method predicts accurate dipole moments for a large collection of molecules, including some with delocalized π-electron systems (with the aug-cc-pVTZ basis

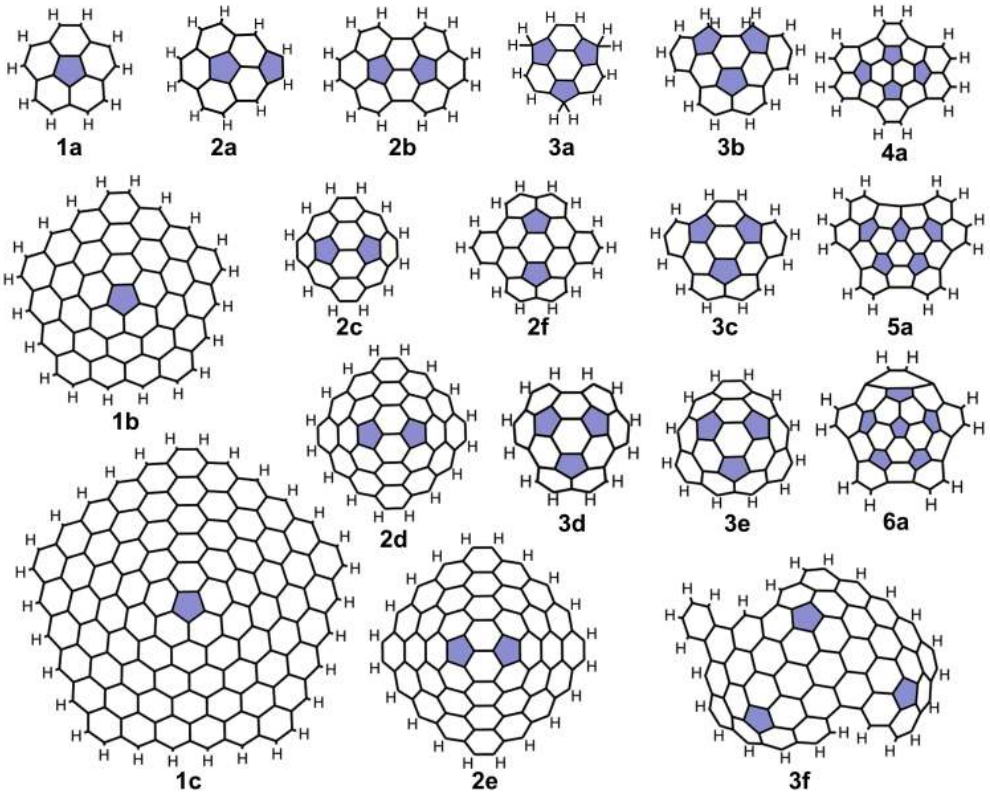

Figure 1: The list of curved arenes considered in this work: corannulene **1a**,[14] dicircumcorannulene **1b** and tricircumcorannulene **1c**,[33] acecorannulene **2a**,[34] [5,5]circulene **2b**,[35] sumanene **3a**,[31] acenaphth[3,2,1,8-fghij]-as-indaceno-[3,2,1,8,7,6-pqrstuv]picene derivatives **3b**, **3c** and **2f**,[32,36] circumtrindene **3d**[37] and penta-benzocorannulene **6a**.[38] Other curved arenes **2c**, **2d**, **2e**, **2f**, **3e**, **4a** and **5a** were also studied. Pentagons are colored for clarity.

set).[44] We compared the dipole moment of corannulene as calculated with this functional to the post-Hartree-Fock method MP2[45] values, Table 1. The geometries were optimized with a variety of basis sets and calculated using the Gaussian 09 software.[46] The dipole moment of corannulene determined experimentally from the Stark effect is 2.071 D.[15] For B3LYP, the dipole moment converged to 2.044 D for the largest basis set (1400 functions) we used. As seen in Table 1, B3LYP yields a reasonably accurate dipole moment even with moderately sized basis sets where MP2 fails.

In order to tackle the geometry optimization of the larger structures we used the B3LYP/6-311+G(d,p) level of theory to optimize the geometry of the structures in Figure 1, with the exception of the largest structures, **1c** and **3f**, where geometry optimization was per-

Table 1: Dipole moment (in debye) of corannulene calculated with B3LYP and MP2 methods, using basis sets with a different number of basis functions, with % deviation from the experimental value of 2.071 D.[15]

Basis set	Function no.	B3LYP dipole		MP2 dipole	
3-21G	200	2.414	(16.6%)	2.777	(34.1%)
6-31G(d)	320	1.722	(16.9%)	2.173	(4.9%)
6-311+G(d,p)	500	2.187	(5.6%)	2.667	(28.8%)
cc-pVTZ	740	1.994	(3.7%)	2.419	(16.8%)
cc-pVQZ	1400	2.044	(1.3%)	–	–

formed using the smaller basis set 3-21G. The electronic structure was then calculated at the B3LYP/cc-pVQZ level of theory for all of the geometry optimized structures. This procedure (a B3LYP/6-311+G(d,p) geometry used for the B3LYP/cc-pVQZ calculation of the electronic structure) led to a dipole moment for corannulene of 2.062 D, differing by 0.45% from the experimental value. This coincidence is in part fortuitous, in view of the 1.3% deviation of the fully geometry-optimized corannulene structure at the cc-pVQZ level of theory from the experimental dipole, Table 1. The obtained dipole moments of all PAHs considered can be found in Table 2. The full geometry-optimized structures and calculated dipole moments are provided in the supplementary information; additional data from the calculation are also made available online.[47]

Two methods were employed to determine the atom-centered multipoles: the atoms in molecules (AIM) approach[48] and the Gaussian distributed multipole analysis (GDMA) method.[49] The AIM approach partitions the atoms into volumes with the heuristic condition $\nabla\rho(\mathbf{r}) = 0$ defining the interfaces between them, where ρ is the electron density. By integration of the charge density (electron density along with the nuclei) over these atomic volumes, the AIM analysis allows the calculation of the atom-centered multipoles up to quadrupole moments. This method produces reasonable values of the atom-centered multipole moments, which are size extensible and independent of the basis set[50] as the decomposition uses the electron density directly as provided by the electronic structure calculation. However, the partitioning and numerical integration are computationally expensive and could not be ap-

plied to the largest carbon structures we study. The GDMA method is of lower computational cost as it provides the atom-centered multipoles directly from the optimized molecular orbital calculations. GDMA makes use of the Gaussian basis functions to readily calculate the multipoles originating from the orbital overlap. These multipoles are then shifted by moving their origin to the nearest atom, and summed to provide the atom-centered multipoles.[49] Further details on the decomposition methods can be found in the supplementary information.

Results and Discussion

Origin of the dipole moment. The dipole of curved arenes could originate from **(i)** a curvature-induced flexoelectric dipole from the polarization of the π bonds in direction normal to the C-skeleton;[21,51–53] **(ii)** the tilt angle of the C–H bonds;[54] **(iii)** charge transfer from the delocalized π-electrons in hexagonal sites to localized states on pentagonal sites[22,55–57] or **(iv)** to localized states at the rim of the PAH.[58] To explore the importance of each of these factors, we first investigated the correlation of the dipole moment to the size of the molecule and the number of pentagons in it. Figure 2 shows the dipole moment as a function of the number of rings N_{rings}. The size dependency of the dipole for fragments of the C-skeleton of a nanocone has been found to be linear with the diameter of the aromatic network.[21] We find a similar linear trend of the dipole as a function of $\sqrt{N_{\text{rings}}}$ (which is proportional to the linear diameter of the fragment), i.e. the dipole moment of hydrogen-passivated curved PAH molecules also scales approximately linearly with diameter (Figure 2, inset). The dipole moment increases with the number of pentagons in the PAH, but it soon saturates after two to three pentagonal rings have been incorporated, which was also found for nanocones.[21] Thus, for curved PAHs with more than two pentagons, the dipole moment depends on the size but not on the number of pentagons.

To illustrate the effect of curvature on the electrostatic potential through the effects (i-

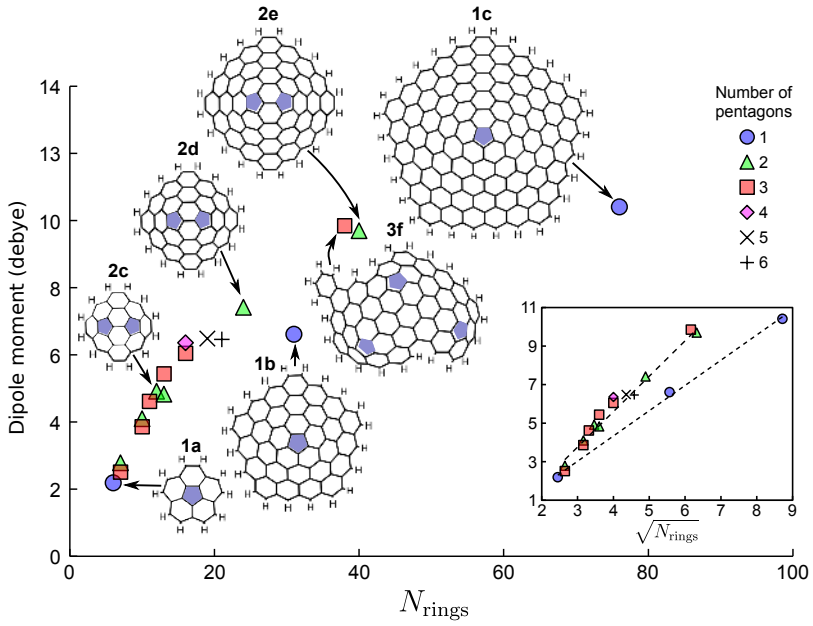

Figure 2: Dipole moment of curved PAH molecules as a function of the number of rings. Inset: Dipole moment as a function of size comparing different numbers of pentagons.

ii), the flexoelectric effect and CH bonds, we compared in Figure 3a-e the potentials created by the flat PAH coronene with one of the curved PAHs, corannulene (**1a**). In both cases, the excess positive charge dominates the potential in the region of the hydrogen atoms and excess negative charge dominates above and below the plane of the aromatic system due to the π-electrons – this distribution provides the large quadrupole moment of these PAHs. A cross section along the zy-plane of the electrostatic potential ϕ demonstrates a significant difference between the flat and curved cases: a normal polarization (relative to the aromatic skeleton) of the π-electron charge is apparent. An additional example is given in Figure S1 in the supplementary information, where the π-electron localization of artificially flattened and relaxed curved corannulenes are compared:[59] in the curved structure, the π bonds at the hub of the molecule are visibly polarized in direction normal to the C-skeleton of the corannulene. The electrostatic π-electron repulsion on the concave side of the molecular bowl leads to increase of the electron density on the convex side, and thus, to the large dipole moment of corannulene (as was observed earlier[60]).

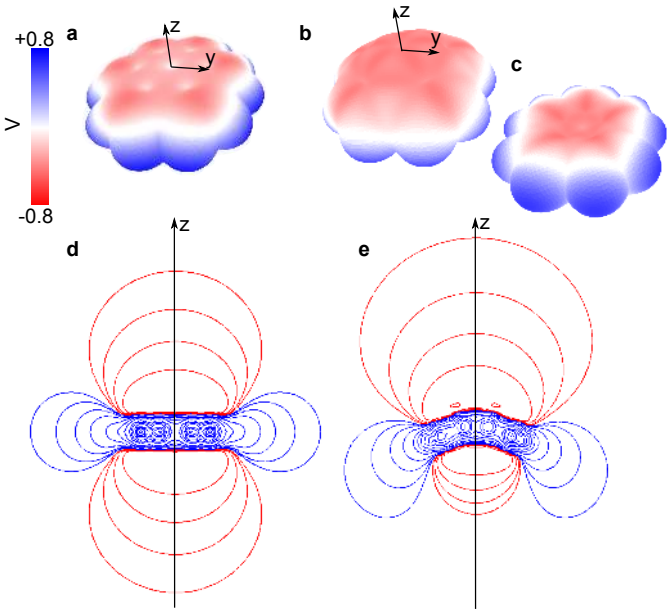

Figure 3: Coronene and corannulene are shown left (a,d) and right (b,c,e). The molecular electrostatic potential was mapped to an isosurface of the electron density (B3LYP/cc-pVQZ, with an isovalue of 0.001 e Å^{-3}) (a,b,c). A two dimensional contour plot of the electrostatic potential through the z-y plane is shown (d,e), with the outermost four contour lines being drawn at ± 0.03, 0.06, 0.1 and 0.2 V.

To illustrate the effects (iii) and (iv) from the localized states near the edge and at the pentagons, in Figure 4a we calculated for molecule **3f** the electron localization function (ELF) – an analysis that has proved useful for curved PAHs.[61] The ELF is a measure of the likelihood of finding two electrons of the same spin in a small region of space. It is defined as[62]

$$\mathrm{ELF}(\mathbf{r}) = \left[1 + \frac{D(\mathbf{r})^2}{D_0(\mathbf{r})^2}\right]^{-1}, \tag{1}$$

where $D(\mathbf{r}) = \tau_\sigma(\mathbf{r}) - |\nabla\rho_\sigma(\mathbf{r})|^2/4\rho_\sigma(\mathbf{r})$ is proportional to the first non-vanishing coefficient in the Taylor expansion (with respect to small $|\mathbf{r}|$) of the spherically averaged conditional pair probability to find a same-spin electron in the vicinity of an electron in the vector-position $\mathbf{r}$; $\tau_\sigma = \sum_i^\sigma |\nabla\psi_i|^2$ is the kinetic energy density, $\rho_\sigma = \sum_i^\sigma \psi_i^*\psi_i$ is the σ-spin probability density and $D_0(\mathbf{r}) = 9.12\rho_\sigma^{5/3}(\mathbf{r})$ is the value for a uniform electron gas. A value of ELF = 1 corresponds to a perfectly localized electron and ELF = 1/2 to a uniform electron gas. Figure 4 shows the iso-ELF surface (iso-value = 0.66), calculated using the Multiwfn

program,[63] within which a region of localized electron pairing occurs. There appears greater localization of the electrons at the pentagonal sites of **3f** (effect (iii)) compared to the hexagonal, cf. Figure 4b. This is a known effect that has been studied in relation to the energetic barrier for inversion of the bowl,[64] where the transition from flattened structure to curved decreases the aromatic delocalization energy (cf. also the supplement). There is also increased localization in the rim region, effect (iv), Figure 4c, in relation to the increased bond order of the C–C bonds at the rim.[58]

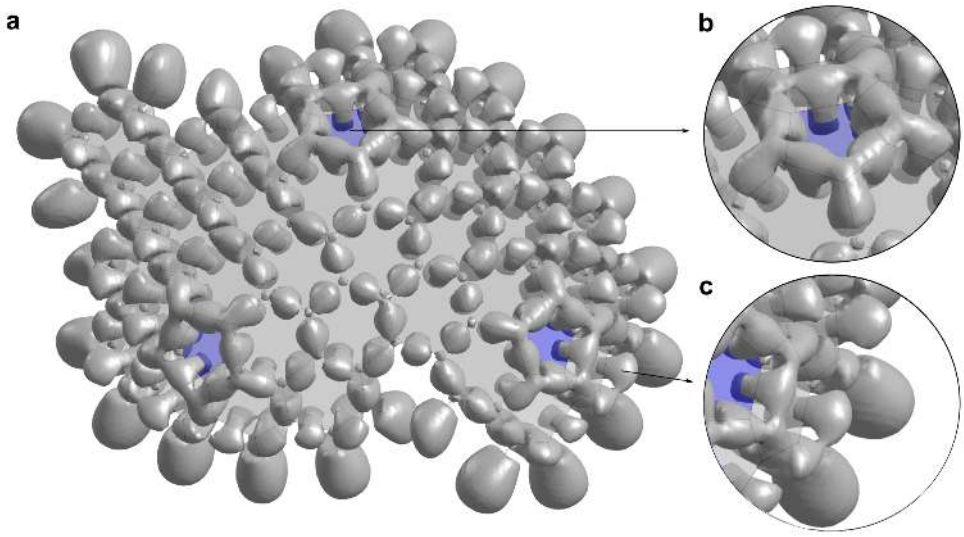

Figure 4: a) Plot of the iso-surfaces of the electron localization function for molecule **3f** at iso-value = 0.66. Pentagonal rings are colored blue and hexagonal rings grey. Insets show b) the localization at pentagonal rings, and c) localization at the rim.

The local flexoelectric dipole moment $\boldsymbol{\mu}_{\text{flex}}$ (per C-site) due to curvature-induced π-bond polarization in direction normal to the C-skeleton has been analyzed previously using a tight binding rehybridization model;[51] linear dependence of $\boldsymbol{\mu}_{\text{flex}}$ with Haddon's pyramidalization angle[65] has been demonstrated:

$$\boldsymbol{\mu}_{\text{flex}} = f_{\theta_{\text{p}}} \theta_{\text{p}} \mathbf{v}_{\pi}. \tag{2}$$

Here, $\mathbf{v}_{\pi}$ is the unit vector collinear with the axis of the π-orbital and points toward the concave side of the PAH, and θ_{p} the pyramidalization angle, a characteristic of the deformation of the carbon skeleton (at each atom center, a plane can be constructed that makes

three equal angles θ_{p} with the adjacent C–C bonds; we refer to this plane as the *pyramidalization plane*). The relation of θ_{p} to the geometry of the molecule is shown in Figure 5b. For small pyramidalization, it is valid that $\theta_{\mathrm{p}} \approx LH/4$, where L is the length of the C–C bond and H is the mean local curvature of the sp^2 skeleton surface;[21] therefore, θ_{p} is essentially a *local* measure of the curvature of the bowl-shaped molecules. The value of the flexoelectric constant $f_{\theta_{\mathrm{p}}}$ of a π-orbital next to a sp^2 carbon atom between three hexagons has been calculated by Kvashnin et al.[21] using electronic structure methods for fullerenes and nanotubes as $f_{\theta_{\mathrm{p}}} = 2.34$ D/rad. Using the approach of these authors, we calculated a similar value of $f_{\theta_{\mathrm{p}}}= 2.35$ D/rad for a (5,5)-nanotube with the B3LYP/cc-pVQZ method we use. This flexoelectric coefficient is obviously unrelated to the localization effects or the CH bond tilt.

The flexoelectric effect dominates the dipole moment of the curved PAHs we consider. This can be shown by neglecting the other three effects leading to polarization. The summation of $\boldsymbol{\mu}_{\mathrm{flex}}$, Eq 2, over all C-sites gives for the total dipole moment $\boldsymbol{\mu}$ of the molecule

$$\boldsymbol{\mu} \approx \sum_{\mathrm{C_{hub}}} \boldsymbol{\mu}_{\mathrm{flex}} = f_{\theta_{\mathrm{p}}} \boldsymbol{\theta}_{\mathrm{tot}}, \tag{3}$$

where we refer to the vector $\boldsymbol{\theta}_{\mathrm{tot}} = \sum_{\mathrm{C_{hub}}} \theta_{\mathrm{p}} \mathbf{v}_{\pi}$ as to the *total pyramidalization* of the molecule. It is a geometric characteristic of the molecular structure (Figure 5b); for small pyramidalization, it can be expressed as $\boldsymbol{\theta}_{\mathrm{tot}} \approx LN_{\mathrm{C_{hub}}} \overline{H\mathbf{v}_{\pi}}/4$, where $N_{\mathrm{C_{hub}}}$ is the number of hub atoms. Thus, $\boldsymbol{\theta}_{\mathrm{tot}}$ is a *global* measure of the curvature of the molecule as a whole, equal within a coefficient to the average mean curvature vector $H\mathbf{v}_{\pi}$ of the sp^2-skeleton. The rim C-atoms (bonded to hydrogen) are neglected in the sum (Eq. 3), with the assumption that the π-electron repulsion leading to the polarization is less effective for the two adjacent π orbitals next to a rim C compared to three π orbitals next to a hub C. We also excluded the sp^3 carbon atoms (having no π-orbitals) in structures **3a** and **3b**. To determine the vector $\mathbf{v}_{\pi}$, we used the POAV2 approach of Haddon,[65] in which six conditions for orthogonality of the

hybridized orbitals of the form $1 + \lambda_i \lambda_j \mathbf{v}_i \cdot \mathbf{v}_j = 0$, where $i, j = 1, 2, 3, \pi$, are used determine the four hybridizations λ_i and to express $\mathbf{v}_\pi$ as a linear combination of the unit vectors $\mathbf{v}_{1,2,3}$ defined by the C–C bonds. Note that this $\mathbf{v}_\pi$ can be quite different from the normal vector to the pyramidalization plane (which is used often as an approximation of $\mathbf{v}_\pi$ within the POAV1 approach[65]). If the contributions to μ of the localization effects and the CH bond tilt are small, the dipole moment of all molecules we investigate must be proportional to $\boldsymbol{\theta}_{\rm tot}$, with proportionality coefficient $f_{\theta_{\rm p}}$. This is indeed the case, as demonstrated in Figure 5a; the linear relationship (Eq. 3) holds with $R^2 = 0.995$ and the value of the linear coefficient is $f_{\theta_{\rm p}} = 2.24 \pm 0.03$ D/rad (all errors are 2σ). This value differs by 4.7% from the one calculated for a nanotube, i.e. more than 95% of the dipole of the curved PAHs considered here is of flexoelectric origin.

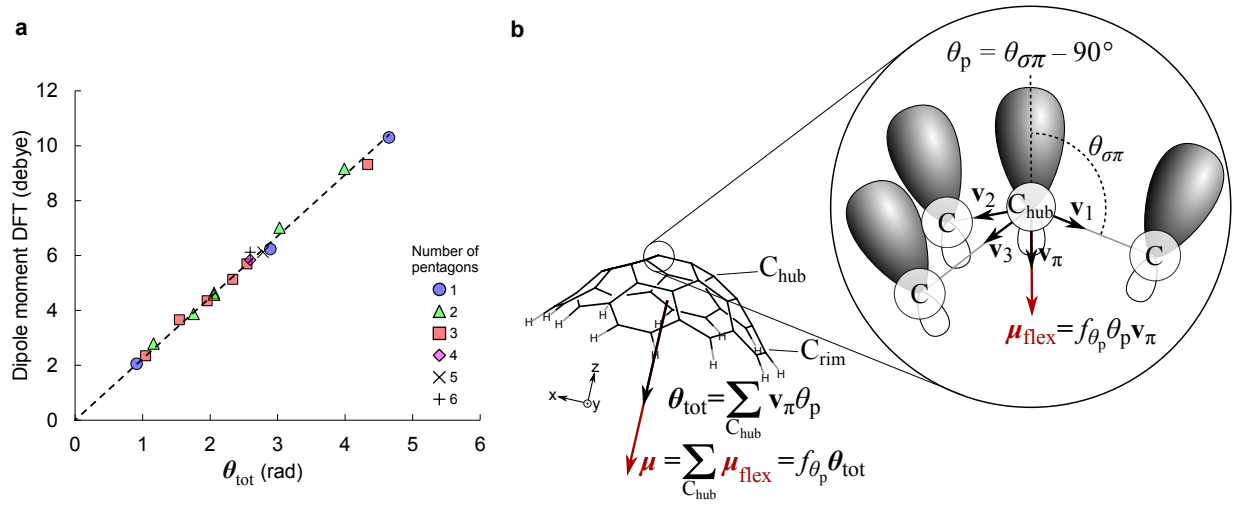

Figure 5: **a)** Values of $\boldsymbol{\theta}_{\rm tot}$ from Eq. 3 (dashed line) compared with the calculated DFT dipole moments for the set of molecules in Figure 1, cf. Table 2. The number of pentagons for each fragment is also indicated. **b)** Illustration of the relation of $\boldsymbol{\theta}_{\rm tot}$ and $\theta_{\rm p}$ to the geometry of the molecule. At each sp^2 carbon, a *pyramidalization plane* can be constructed that makes equal angles ($\theta_{\rm p}$) with the three adjacent C–C bonds. The normal to this plane is approximately colinear with the π orbital axis. The angle $\theta_{\sigma\pi}$ in the figure is the one between the C–C bonds and the normal to the pyramidalization plane.

The contribution of the other three effects is surprisingly small. We attempted to elaborate the geometrical model Eq. 3 by including the contribution of the C–H bond dipole (ii) and the rim localization (iv), and also by allowing for different values of $f_{\theta_{\rm p}}$ for carbon

in pentagons and at the rim. However, due to the complete domination of the flexoelectric effect and to efficient compensation of the other polarization sources, the respective effects cannot be decoupled in this manner. Qualitatively, by considering the direction of the effects (ii-iv) relative to the flexoelectric dipole (i), one can conclude that the observed 4.7% reduction of the flexoelectric coefficient is mostly due to the neglected rim localization effect (iv). (The dipoles due to the C–H bond tilt (ii) and to the pentagon localization (iii) are in the same direction as the flexoelectric dipole – plus pole towards the concave side – and would lead to a larger effective f_{θ_p} value in Eq. 3.) However, even this conclusion is uncertain as the error in the calculation of the π-electron flexoelectric effect is probably of the same order of magnitude as the combined result of all other effects: a small additional π-electron flexoelectric effect can be expected from (i) the rim atoms we neglected, and from (ii) the asymmetric deformation at the pentagon C-atoms (where torsional misalignment of the π orbitals is present, similar to the one studied by Nikiforov et al.[53] in relation to nanotube strain energy – it may affect $\boldsymbol{\mu}_\mathrm{flex}$). The simulations of flattened corannulene in the supplementary information confirm that the linear flexoelectric effect dominates the polarization, and also indicate that the success of Eq. 3 is due to fortuitous cancellation of effects (leading to a slight non-linear dependence of the dipole moment on θ_p at small pyramidalization angles).

To conclude, Eq. 3 allows the calculation of the dipole moment of a curved arene from our list with an average error of 2.3±1.9%, which is a satisfactory accuracy in view of the expected error of the DFT values (cf. Table 2). A component-by-component comparison between the DFT dipole with the one calculated via Eq. 3 is given in Table 3 for the large asymmetric structure 3f (showing the worst match to Eq. 3 from those in Table 2): the difference in magnitude is 4% and the difference in direction is 6°.

Table 2: Dipole moment and pyramidalization of the curved aromatic hydrocarbons in Figure 1: DFT dipole values (B3LYP method) compared with the model Eq. 3 and total and maximum pyramidalization angles.

Molecule	DFT dipole μ [D]	max. pyr. angle $\max(\theta_\mathrm{p})$ [°]	total pyr. $\lvert\boldsymbol{\theta}_\mathrm{tot}\rvert$ $\sum_{\mathrm{C_{hub}}} \theta_\mathrm{p}\mathbf{v}_\pi$ [rad]	flexoel. dipole $\sum_{\mathrm{C_{hub}}} \boldsymbol{\mu}_\mathrm{flex}$ [D]
1a	2.06	8.34	0.909	2.03
1b	6.24	10.48	2.89	6.46
1c	10.30	10.59	4.65	10.39
2a	2.79	10.99	1.16	2.59
2b	3.87	11.23	1.75	3.92
2c	4.63	11.63	2.06	4.60
2d	7.01	11.91	3.03	6.76
2e	9.15	11.59	3.99	8.92
2f	4.57	10.65	2.06	4.60
3a	2.34	8.85	1.04	2.33
3b	3.66	12.51	1.54	3.45
3c	4.35	12.35	1.96	4.37
3d	5.13	12.08	2.33	5.21
3e	5.70	12.17	2.54	5.69
3f	9.32	10.64	4.33	9.69
4a	5.84	12.52	2.59	5.80
5a	6.12	12.28	2.78	6.22
6a	6.12	12.09	2.59	5.80

Distributed multipole expansion. Curved aromatic structures play a role in numerous technologically relevant processes and the interest towards modelling the interactions within these materials is growing. One such process of interest to us is the role of the curved PAHs' dipole in soot formation. A strong correlation is known to exist between soot formation and chemi-ions in a flame,[66] but Chen and Wang recently calculated binding energies between flat PAH and flame chemi-ions that are not strong enough to stabilize anything larger than a dimer.[67] One can expect the situation to be qualitatively different with curved PAHs due to strong ion-dipole interaction, which might be involved in stabilising clusters of PAHs, but an appropriate force field is required to study this case. A second example is the adsorption in microporous carbon. The effect of the curvature has been explored, e.g. for hydrogen absorption, which is enhanced on corannulene due to a permanent dipole-induced dipole interaction modeled with molecular dynamics via modification of the van der

Waals parameters of the force field.[68] Obviously, for adsorption of *polar* molecules on microporous carbon, a strong directional permanent dipole-permanent dipole interaction will control the process – in this case, an effective van der Waals model of the flexoelectric dipole interactions is inapplicable. The strained pentagon presents a binding site for ions as well[69] (which is probably the reason why corannulene allows for supercharging of lithium in battery applications[70]) and force fields are also required for this case.

The most common representation of the charge distribution in a molecule used in force fields is an ensemble of atom-centered point charges. However, this model is unsuitable for curved PAHs, where the most long-ranged interaction is due to the π-electron flexoelectric dipole that cannot be represented with atom-centered point charges. Therefore, we will now investigate the capability of a distributed multipole[49] description of the electrostatic potential of curved PAHs.

The expansion of the electrostatic potential in an ensemble of multipole centers (a set of atom-centered charge, dipole, quadrupole, etc.) is not unique – different sets of values of the multipoles at each center can produce the same total potential, and all decomposition methods are based on heuristic assumptions of how the electron density is separated between the atoms; therefore, no strict physical meaning should be ascribed to the values of the multipoles in a distributed multipole expansion. Nevertheless, we sought a decomposition that not only describes the electrostatic potential outside the van der Waals surface correctly, but is also physically reasonable. We tested two methods which are commonly employed for the decomposition: the Gaussian distributed multipole analysis (GDMA)[49] and the atoms-in-molecules (AIM) approach.[48] The advantage of the AIM approach is that the electron density itself is partitioned and then integrated to yield the multipoles in the atomic basins, making the decomposition independent of the basis set of molecular orbitals used and of the system size.[50] On the other hand, GDMA computes the multipoles directly from the Gaussian basis functions, is fast even for the largest structures we studied, and is more widely used (GDMA point multipoles have been integrated into molecular dynamics packages such

as AMOEBA, CHARMM and DL_MULTI). Two variants of GDMA were employed: one with rank 2 multipoles (point charge-dipole-quadrupole) on every atom, to which we refer as GDMA(C_2H_2), and another with rank 2 multipoles on every carbon but only a point charge (rank 0 restriction) on every hydrogen, GDMA(C_2H_0). For the PAHs in Figure 1, both methods produce a total dipole moment of magnitude within ±0.002 D of the exact μ that follows from the electronic structure calculations. An example is given in Table 3 for the asymmetric PAH **3f**: the component-by-component comparison of the total dipole for the GDMA(C_2H_0) multipole expansion and the DFT shows that the GDMA method reproduces all components effectively. GDMA(C_2H_0) and AIM agreed well in all cases. However, the larger structures had significant divergence between GDMA(C_2H_2) and AIM (discussed further in the supplementary information, section 2).

Table 3: Dipole moment components (in debye) of molecule 3f calculated with DFT, Eq. 3 and GDMA(C_2H_0).

	μ_x	μ_y	μ_z
DFT	-1.183	-0.763	-9.211
Eq. 3	-0.181	-0.742	-9.660
GDMA(C_2H_0)	-1.085	-0.789	-9.219

Figure 6a-b shows the GDMA(C_2H_0) distributed point dipoles and monopoles with the geometry of molecule **3f**. The C-centered dipole moments range between 0.11 and 0.79 D in magnitude. The procedure computes a large dipole at each rim carbon atom, in the direction of the C–H bond with the positive pole pointing toward the hub. This polarization reflects mostly the localized states at the rim of the PAH (increased bond orders and electron density near the rim compared to the hub,[58] effect (iv)). In the GDMA(C_2H_0) decomposition, the polarization of the C–H bonds (and effect (ii)) is reflected by the partial charges at the C and H atoms. From the dipole at each pyramidalized hub C-atom and the local θ_{p}, we obtain "local values" for the flexoelectric coefficient $f_{\theta_{\mathrm{p}}}$ in the range 2.24–2.27 D/rad, that coincide with the "averaged" $f_{\theta_{\mathrm{p}}}$ value in Eq. 3 and Figure 5a. The largest contributors to the net dipole moment are the pentagonal carbon atoms which are the most heavily

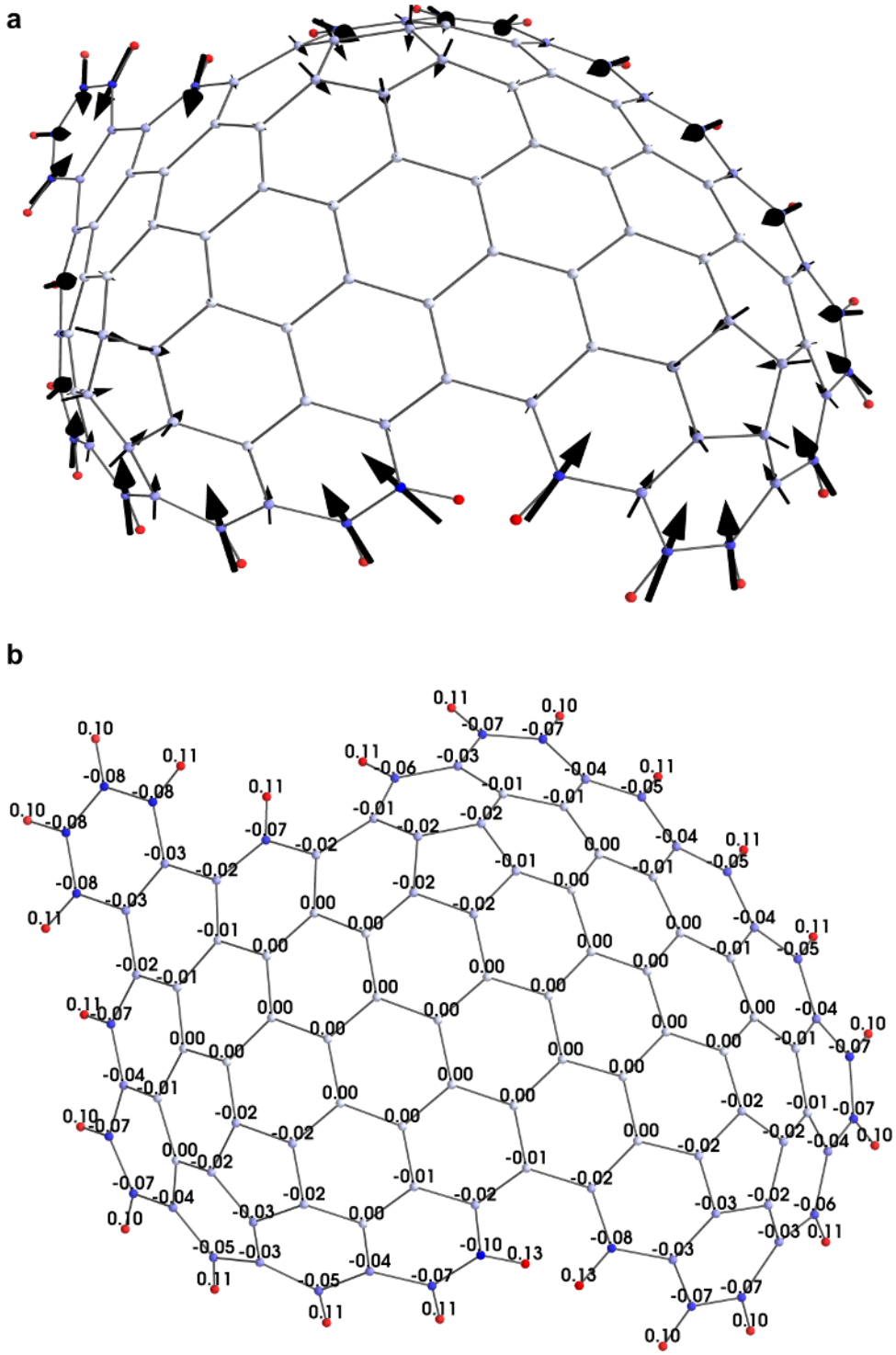

Figure 6: GDMA dipoles a) and partial charges b) for the molecule **3f** with the dipoles shown as vectors and partial charge values printed at the atomic sites.

pyramidalized. The total dipole moment per pentagonal ring (defined as the vector sum of the GDMA(C_2H_0) dipoles of all atoms in the pentagon) was found to be of magnitude 1.76±0.03 D. Finally, in Figure 6b, the partial charges at the pentagonal carbon atoms are found to range between -0.01 and -0.03 e and each pentagon contains a total charge of -0.09±0.02 e (effect (iii)). This value is slightly less than what has previously been predicted for the pentagonal charge accumulation in nanotube end caps, -0.013 e (calculated using the PBE density functional, with plane wave basis functions up of 25 and 225 Ry for the valance and charge density, respectively).[22,56] Thus, all four polarization effects are well represented by the GDMA(C_2H_0) distributed multipole expansion.

Figure 7a-d shows the electrostatic potential on the zy plane outside the van der Waals surface of corannulene for two different multipole decompositions: 7c is GDMA(C_2H_0) and 7a is the standard point charge description as obtained by the Merz-Kollman (MK) scheme. Figures 7b and d show the difference between these potentials and the exact DFT potential given in Figure 3 (we used the procedure of Kramer et al.[71]). A significant divergence between the point charge ensemble's potential and the DFT potential is evident, especially near the pentagonal carbon atoms where the flexoelectric dipole is large (Figure 7b). On the other hand, the GDMA(C_2H_0) representation is accurate (Figure 7d). In order to quantify the differences, the molecular electrostatic potential was calculated at the electron density isosurface 0.002 $e/Å^3$ (near the interaction surface of molecular pairs). For the point charge model, the average difference between the DFT and the model potentials at this surface was 36%. The error was reduced to 2.6% for the GDMA(C_2H_0) distributed multipole representation. An additional problem of the MK description is that the total dipole moment of the point charge ensemble is 1.73 D, a value reduced by 16% compared with the DFT dipole. Finally, GDMA(C_2H_0) also produces reasonably accurate molecular quadrupole moments: Q_{xx}=6.10/6.80, Q_{yy}=6.09/6.79 and Q_{zz}=-12.19/-13.59 DFT/GDMA(C_2H_0) (in a.u.).

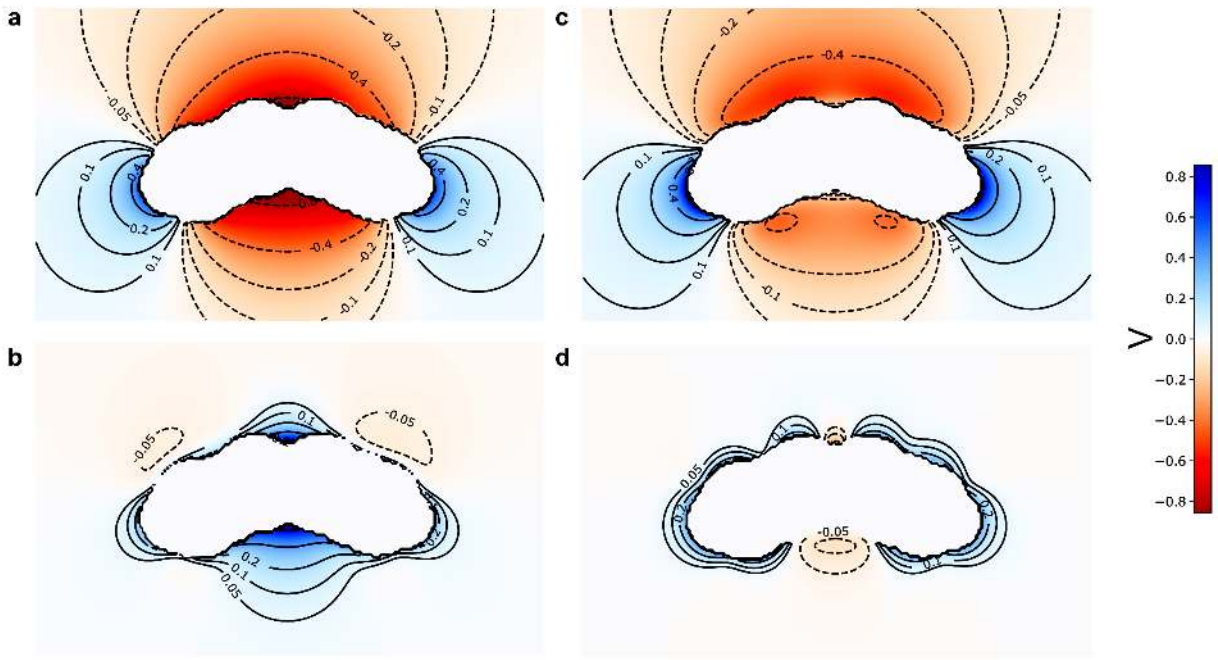

Figure 7: Electrostatic potential along the zy plane for corannulene (**1a**) calculated from a) the distributed point charge model obtained by the MK scheme, and c) the GDMA(C_2H_0) multipole representation. Potential maps of the difference between these potentials and the DFT result in Figure 3e are given for the distributed point charge (b) and for the multipole (d) models.

Conclusion

The dipole moment μ of 18 curved aromatic molecules has been computed and was shown to reach significant values (2-10 D). The main contribution to this moment was shown to stem from the π-orbital flexoelectric polarization: μ of all these molecules can be calculated with 95% accuracy using a standard linear model for the dependence of the flexoelectric effect on the pyramidalization at each carbon atom. Gaussian distributed multipole expansion, restricted to rank 2 at the carbon atoms and rank 0 at the hydrogens – GDMA(C_2H_0) – has been shown to reproduce the electrostatic potential of the curved arenes with sufficient accuracy. The distributed multipole analysis has been previously applied to flat PAH molecules by Totton et al.,[72,73] who found it improved on point charge models, allowing the reproduction of the second virial coefficient of benzene, and highlighting the importance of the

quadrupole moment terms.[73] Yet, for dimers of flat PAH molecules, a point charge distribution was found sufficient for developing an accurate force field (iso-PAHAP).[72,73] Here we show that for curved PAHs, this is not the case. The common atom-centered point charge models fail to correctly reproduce the π-electron flexoelectric dipole moment, which controls the long range potential and contributes significantly to the short range interactions. As a result, the electrostatic potential distribution (which represents the main component of the PAH-ion interaction) is highly inaccurate for point charge models, Figure 7. Therefore, atom-centered point charge ensembles are inapplicable as a basis for force fields for molecular dynamic simulations of curved PAHs. Thus, this work provides a starting point for correctly describing the electrostatic field in force fields around curved PAHs for many different carbon materials.

Acknowledgement

This project is supported by the National Research Foundation (NRF), Prime Minister's Office, Singapore under its Campus for Research Excellence and Technological Enterprise (CREATE) program. The authors thank Dr. Grant McIntosh, University of Auckland, for his aid in performing the strained corannulene calculations.

Supporting Information Available

Calculations of constrained geometry optimized corannulene. AIM and GDMA atom centered multipoles comparison. Geometry optimized structures of all curved aromatics. This material is available free of charge via the Internet at `http://pubs.acs.org/`.

References

(1) Yapp, E. K. Y.; Wells, C. G.; Akroyd, J.; Mosbach, S.; Xu, R.; Kraft, M. Modelling (PAH) curvature in laminar premixed flames using a detailed population balance model. *Combust. Flame* **2017**, *176*, 172 – 180.

(2) Singh, R.; Frenklach, M. A mechanistic study of the influence of graphene curvature on the rate of high-temperature oxidation by molecular oxygen. *Carbon* **2016**, *101*, 203–212.

(3) Whitesides, R.; Frenklach, M. Detailed kinetic Monte Carlo simulations of graphene-edge growth. *The J. Phys. Chem. A* **2010**, *114*, 689–703.

(4) Harris, P. J. F.; Liu, Z.; Suenaga, K. Imaging the atomic structure of activated carbon. *J. Physics: Condens. Matter* **2008**, *20*, 362201.

(5) Richter, H.; Labrocca, A. J.; Grieco, W. J.; Taghizadeh, K.; Lafleur, A. L.; Howard, J. B. Generation of Higher Fullerenes in Flames. *J. Phys. Chem. B* **1997**, *101*, 1556–1560.

(6) Lafleur, A. L.; Howard, J. B.; Marr, J. A.; Yadav, T. Proposed fullerene precursor corannulene identified in flames both in the presence and absence of fullerene production. *The J. Phys. Chem.* **1993**, *97*, 13539–13543.

(7) Botero, M. L.; Adkins, E. M.; González-Calera, S.; Miller, H.; Kraft, M. PAH structure analysis of soot in a non-premixed flame using high-resolution transmission electron microscopy and optical band gap analysis. *Combust. Flame* **2016**, *164*, 250–258.

(8) Su, D. S.; Jentoft, R. E.; Müller, J. O.; Rothe, D.; Jacob, E.; Simpson, C. D.; Tomović, Ž.; Müllen, K.; Messerer, A.; Pöschl, U. et al. Microstructure and oxidation behaviour of Euro IV diesel engine soot: a comparative study with synthetic model soot substances. *Catal. Today* **2004**, *90*, 127–132.

(9) Harris, P. J. F. Fullerene-related structure of commercial glassy carbons. *Philos. Mag.* **2004**, *84*, 3159–3167.

(10) Terzyk, A. P.; Furmaniak, S.; Harris, P. J. F.; Gauden, P. A.; Włoch, J.; Kowalczyk, P.; Rychlicki, G. How realistic is the pore size distribution calculated from adsorption isotherms if activated carbon is composed of fullerene-like fragments? *Phys. Chem. Chem. Phys.* **2007**, *9*, 5919.

(11) Terzyk, A. P.; Furmaniak, S.; Gauden, P. A.; Harris, P. J.; Kowalczyk, P. *Novel Carbon Adsorbents*; Elsevier, 2012; pp 61–104.

(12) Wu, X. Z.; Yao, Y. R.; Chen, M. M.; Tian, H. R.; Xiao, J.; Xu, Y. Y.; Lin, M. S.; Abella, L.; Tian, C. B.; Gao, C.-L. et al. Formation of Curvature Subunit of Carbon in Combustion. *J. Am. Chem. Soc.* **2016**, *138*, 9629–9633.

(13) You, X.; Whitesides, R.; Zubarev, D.; Lester, W. A.; Frenklach, M. Bay-capping reactions: Kinetics and influence on graphene-edge growth. *Proc. Combust. Inst.* **2011**, *33*, 685–692.

(14) Lawton, R. G.; Barth, W. E. Synthesis of corannulene. *J. Am. Chem. Soc.* **1971**, *93*, 1730–1745.

(15) Lovas, F. J.; McMahon, R. J.; Grabow, J. U.; Schnell, M.; Mack, J.; Scott, L. T.; Kuczkowski, R. L. Interstellar chemistry: A strategy for detecting polycyclic aromatic hydrocarbons in space. *J. Am. Chem. Soc.* **2005**, *127*, 4345–4349.

(16) Shostak, S. L.; Ebenstein, W. L.; Muenter, J. S. The dipole moment of water. I. Dipole moments and hyperfine properties of H_2O and HDO in the ground and excited vibrational states. *The J. Chem. Phys.* **1991**, *94*, 5875.

(17) Steinberg, B. D.; Jackson, E. A.; Filatov, A. S.; Wakamiya, A.; Petrukhina, M. A.; Scott, L. T. Aromatic π-Systems More Curved Than C_{60}. The Complete Family of All

Indenocorannulenes Synthesized by Iterative Microwave-Assisted Intramolecular Arylations. *J. Am. Chem. Soc.* **2009**, *131*, 10537–10545.

(18) Filatov, A. S.; Scott, L. T.; Petrukhina, M. A. π-π Interactions and Solid State Packing Trends of Polycyclic Aromatic Bowls in the Indenocorannulene Family: Predicting Potentially Useful Bulk Properties. *Cryst. Growth & Des.* **2010**, *10*, 4607–4621.

(19) Ge, M.; Sattler, K. Observation of fullerene cones. *Chem. Phys. Lett.* **1994**, *220*, 192–196.

(20) Krishnan, A.; Dujardin, E.; Treacy, M. M. J.; Hugdahl, J.; Lynum, S.; Ebbesen, T. W. Graphitic cones and the nucleation of curved carbon surfaces. *Nat.* **1997**, *388*, 451–454.

(21) Kvashnin, A. G.; Sorokin, P. B.; Yakobson, B. I. Flexoelectricity in Carbon Nanostructures: Nanotubes, Fullerenes, and Nanocones. *J. Phys. Chem. Lett.* **2015**, *6*, 2740–2744.

(22) Otani, M.; Okada, S.; Okamoto, Y. Intrinsic dipole moment on the capped carbon nanotubes. *Phys. Rev. B - Condens. Matter Mater. Phys.* **2009**, *80*, 4–6.

(23) Knaapila, M.; Rømoen, O. T.; Svåsand, E.; Pinheiro, J. P.; Martinsen, Ø. G.; Buchanan, M.; Skjeltorp, A. T.; Helgesen, G. Conductivity Enhancement in Carbon Nanocone Adhesive by Electric Field Induced Formation of Aligned Assemblies. *ACS Appl. Mater. & Interfaces* **2011**, *3*, 378–384.

(24) Li, W.; Zhou, X.; Tian, W. Q.; Sun, X. A new scheme for significant enhancement of the second order nonlinear optical response from molecules to ordered aggregates. *Phys. Chem. Chem. Phys.* **2013**, *15*, 1810.

(25) Wang, B. T.; Petrukhina, M. A.; Margine, E. R. Electronic transport properties of selected carbon π-bowls with different size, curvature and solid state packing. *Carbon* **2015**, *94*, 174–180.

(26) Bauert, T.; Zoppi, L.; Koller, G.; Garcia, A.; Baldridge, K. K.; Ernst, K. H. Large induced interface dipole moments without charge transfer: Buckybowls on metal surfaces. *J. Phys. Chem. Lett.* **2011**, *2*, 2805–2809.

(27) Gerald, R.; Johnson, C.; Rathke, J.; Klingler, R.; Sandí, G.; Scanlon, L. ^{7}Li NMR study of intercalated lithium in curved carbon lattices. *J. Power Sources* **2000**, *89*, 237–243.

(28) Yoshizawa, N.; Yamada, Y.; Shiraishi, M. TEM lattice images and their evaluation by image analysis for activated carbons with disordered microtexture. *J. Mater. Sci.* **1998**, *33*, 199–206.

(29) Xu, Z.; Liang, Z.; Ding, F. Isomerization of sp^2-hybridized carbon nanomaterials: structural transformation and topological defects of fullerene, carbon nanotube, and graphene. *Wiley Interdiscip. Rev. Comput. Mol. Sci.* **2017**, *7*, e1283.

(30) Stein, S. E.; Fahr, A. High-temperature stabilities of hydrocarbons. *The J. Phys. Chem.* **1985**, *89*, 3714–3725.

(31) Sakurai, H. A Synthesis of Sumanene, a Fullerene Fragment. *Sci.* **2003**, *301*, 1878–1878.

(32) Wu, T. C.; Hsin, H. J.; Kuo, M. Y.; Li, C. H.; Wu, Y. T. Synthesis and Structural Analysis of a Highly Curved Buckybowl Containing Corannulene and Sumanene Fragments. *J. Am. Chem. Soc.* **2011**, *133*, 16319–16321.

(33) Dias, J. R. Resonance Topology of Fluoranthenoid/Fluorenoid Hydrocarbons and Related Systems. *Polycycl. Aromat. Compd.* **2011**, *31*, 48–60.

(34) Abdourazak, A. H.; Sygula, A.; Rabideau, P. W. "Locking" the bowl-shaped geometry of corannulene: cyclopentacorannulene. *J. Am. Chem. Soc.* **1993**, *115*, 3010–3011.

(35) Rabideau, P. W.; Abdourazak, A. H.; Folsom, H. E.; Marcinow, Z.; Sygula, A.; Sygula, R. Buckybowls: Synthesis and ab Initio Calculated Structure of the First Semibuckminsterfullerene. *J. Am. Chem. Soc.* **1994**, *116*, 7891–7892.

(36) Chen, D.; Totton, T. S.; Akroyd, J. W. J.; Mosbach, S.; Kraft, M. Size-dependent melting of polycyclic aromatic hydrocarbon nano-clusters: A molecular dynamics study. *Carbon* **2014**, *67*, 79–91.

(37) Scott, L. T.; Bratcher, M. S.; Hagen, S. Synthesis and Characterization of a $C_{36}H_{12}$ Fullerene Subunit. *J. Am. Chem. Soc.* **1996**, *118*, 8743–8744.

(38) Sastry, G. N.; Jemmis, E. D.; Mehta, G.; Shah, S. R. Synthetic strategies towards C_{60}. Molecular mechanics and MNDO study on sumanene and related structures. *Journal of the Chemical Society, Perkin Transactions 2* **1993**, 1867.

(39) Lee, C.; Yang, W.; Parr, R. G. Development of the Colle-Salvetti correlation-energy formula into a functional of the electron density. *Phys. Rev. B* **1988**, *37*, 785–789.

(40) Becke, A. D. Density-functional thermochemistry. III. The role of exact exchange. *The J. Chem. Phys.* **1993**, *98*, 5648.

(41) Stephens, P. J.; Devlin, F. J.; Chabalowski, C. F.; Frisch, M. J. Ab Initio Calculation of Vibrational Absorption and Circular Dichroism Spectra Using Density Functional Force Fields. *The J. Phys. Chem.* **1994**, *98*, 11623–11627.

(42) Petrukhina, M. A.; Andreini, K. W.; Mack, J.; Scott, L. T. X-ray quality geometries of geodesic polyarenes from theoretical calculations: What levels of theory are reliable? *J. Org. Chem.* **2005**, *70*, 5713–5716.

(43) Grabowsky, S.; Weber, M.; Chen, Y. S.; Lentz, D.; Schmidt, B. M.; Hesse, M.; Luger, P. Electron density of corannulene from synchrotron data at 12 K, comparison with fullerenes. *Zeitschrift fur Naturforschung - Sect. B J. Chem. Sci.* **2010**, *65*, 452–460.

(44) Hickey, A. L.; Rowley, C. N. Benchmarking Quantum Chemical Methods for the Calculation of Molecular Dipole Moments and Polarizabilities. *The J. Phys. Chem. A* **2014**, *118*, 3678–3687.

(45) Möller, C.; Plesset, M. S. Note on an Approximation Treatment for Many-Electron Systems. *Phys. Rev.* **1934**, *46*, 618–622.

(46) Frisch, M. J.; Trucks, G. W.; Schlegel, H. B.; Scuseria, G. E.; Robb, M. A.; Cheeseman, J. R.; Scalmani, G.; Barone, V.; Petersson, G. A.; Nakatsuji, H. et al. Gaussian 09, Revision A 02.

(47) Molhub. `http://como.cheng.cam.ac.uk/molhub`.

(48) Bader, R. F. *Atoms in molecules*; Clarendon Press, 1994.

(49) Stone, A. *The Theory of Intermolecular Forces*; Oxford University Press, 2013.

(50) Matta, C. F., Boyd, R. J., Eds. *The Quantum Theory of Atoms in Molecules*; Wiley-VCH Verlag GmbH & Co. KGaA: Weinheim, Germany, 2007.

(51) Dumitrică, T.; Landis, C. M.; Yakobson, B. I. Curvature-induced polarization in carbon nanoshells. *Chem. Phys. Lett.* **2002**, *360*, 182–188.

(52) Kalinin, S. V.; Meunier, V. Electronic flexoelectricity in low-dimensional systems. *Phys. Rev. B* **2008**, *77*, 1–4.

(53) Nikiforov, I.; Dontsova, E.; James, R.; Dumitrică, T. Tight-binding theory of graphene bending. *Phys. Rev. B* **2014**, *89*, 155437.

(54) Wang, W.; Li, Z. Potential barrier of graphene edges. *J. Appl. Phys.* **2011**, *109*, 114308.

(55) Carroll, D.; Redlich, P.; Ajayan, P.; Charlier, J.; Blase, X.; De Vita, A.; Car, R. Electronic Structure and Localized States at Carbon Nanotube Tips. *Phys. Rev. Lett.* **1997**, *78*, 2811–2814.

(56) Vita, A. D.; Charlier, J.; Blase, X.; Car, R. Electronic structure at carbon nanotube tips. *Appl. Phys. A* **1999**, *68*, 283–286.

(57) An, B.; Fukuyama, S.; Yokogawa, K.; Yoshimura, M.; Egashira, M.; Korai, Y.; Mochida, I. Single pentagon in a hexagonal carbon lattice revealed by scanning tunneling microscopy. *Appl. Phys. Lett.* **2001**, *78*, 3696–3698.

(58) Yang, H.; Mayne, A. J.; Boucherit, M.; Comtet, G.; Dujardin, G.; Kuk, Y. Quantum interference channeling at graphene edges. *Nano Lett.* **2010**, *10*, 943–947.

(59) Martin, J. W.; McIntosh, G. J.; Arul, R.; Oosterbeek, R. N.; Kraft, M.; Söhnel, T. Giant fullerene formation through thermal treatment of fullerene soot. *Carbon* **2017**, *125*, 132–138.

(60) Grimme, S.; Antony, J.; Schwabe, T.; Mück-Lichtenfeld, C. Density functional theory with dispersion corrections for supramolecular structures, aggregates, and complexes of (bio)organic molecules. *Org. & Biomol. Chem.* **2007**, *5*, 741–758.

(61) Mebs, S.; Weber, M.; Luger, P.; Schmidt, B. M.; Sakurai, H.; Higashibayashi, S.; Onogi, S.; Lentz, D. Experimental electron density of sumanene, a bowl-shaped fullerene fragment; comparison with the related corannulene hydrocarbon. *Org. & Biomol. Chem.* **2012**, *10*, 2218.

(62) Becke, A. D.; Edgecombe, K. E. A simple measure of electron localization in atomic and molecular systems. *The J. Chem. Phys.* **1990**, *92*, 5397–5403.

(63) Lu, T.; Chen, F. Multiwfn: a multifunctional wavefunction analyzer. *J. Comput. Chem.* **2012**, *33*, 580–592.

(64) Dobrowolski, M. A.; Ciesielski, A.; Cyrański, M. K. On the aromatic stabilization of corannulene and coronene. *Phys. Chem. Chem. Phys.* **2011**, *13*, 20557.

(65) Haddon, R. C. Hybridization and the orientation and alignment of π-orbitals in non-planar conjugated organic molecules: π-orbital axis vector analysis (POAV2). *J. Am. Chem. Soc.* **1986**, *108*, 2837–2842.

(66) Calcote, H. F.; Olson, D. B.; Keil, D. G. Are ions important in soot formation? *Energy & Fuels* **1988**, *2*, 494–504.

(67) Chen, D.; Wang, H. Cation-π Interactions between Flame Chemi-ions and Aromatic Compounds. *Energy & Fuels* **2017**, *31*, 2345–2352.

(68) Scanlon, L. G.; Balbuena, P. B.; Zhang, Y.; Sandi, G.; Back, C. K.; Feld, W. A.; Mack, J.; Rottmayer, M. A.; Riepenhoff, J. L. Investigation of corannulene for molecular hydrogen storage via computational chemistry and experimentation. *J. Phys. Chem. B* **2006**, *110*, 7688–7694.

(69) Vijay, D.; Sakurai, H.; Subramanian, V.; Sastry, G. N. Where to bind in buckybowls? The dilemma of a metal ion. *Phys. Chem. Chem. Phys.* **2012**, *14*, 3057.

(70) Zabula, A. V.; Filatov, A. S.; Spisak, S. N.; Rogachev, A. Y.; Petrukhina, M. A. A Main Group Metal Sandwich: Five Lithium Cations Jammed Between Two Corannulene Tetraanion Decks. *Sci.* **2011**, *333*, 1008–1011.

(71) Kramer, C.; Gedeck, P.; Meuwly, M. Atomic multipoles: Electrostatic potential fit, local reference axis systems, and conformational dependence. *J. Comput. Chem.* **2012**, *33*, 1673–1688.

(72) Totton, T. S.; Misquitta, A. J.; Kraft, M. A First Principles Development of a General Anisotropic Potential for Polycyclic Aromatic Hydrocarbons. *J. Chem. Theory Comput.* **2010**, *6*, 683–695.

(73) Totton, T. S.; Misquitta, A. J.; Kraft, M. Assessing the Polycyclic Aromatic Hydrocarbon Anisotropic Potential with Application to the Exfoliation Energy of Graphite. *The J. Phys. Chem. A* **2011**, *115*, 13684–13693.

Graphical TOC Entry